

# NAVAL POSTGRADUATE SCHOOL

Monterey, California



## THESIS

### HIGH FREQUENCY CHARACTERIZATION OF THE GSANGER LM0202P ELECTRO-OPTIC MODULATOR

by  
John R Tucker

December, 1996

Thesis Advisors:

S. Gnanalingam  
D. Scott Davis  
Andrés Larraza

19971030 021

Approved for public release; distribution is unlimited.

REPORT DOCUMENTATION PAGE			Form Approved OMB No. 0704-0188	
Public reporting burden for this collection of information is estimated to average 1 hour per response, including the time for reviewing instruction, searching existing data sources, gathering and maintaining the data needed, and completing and reviewing the collection of information. Send comments regarding this burden estimate or any other aspect of this collection of information, including suggestions for reducing this burden, to Washington Headquarters Services, Directorate for Information Operations and Reports, 1215 Jefferson Davis Highway, Suite 1204, Arlington, VA 22202-4302, and to the Office of Management and Budget, Paperwork Reduction Project (0704-0188) Washington DC 20503.				
1. AGENCY USE ONLY (Leave blank)	2. REPORT DATE December 1996.	3. REPORT TYPE AND DATES COVERED Master's Thesis		
4. High Frequency Characterization of the Gsanger LM0202P Electro-Optic Modulator		5. FUNDING NUMBERS		
6. AUTHOR(S) Tucker, John R.				
7. PERFORMING ORGANIZATION NAME(S) AND ADDRESS(ES) Naval Postgraduate School Monterey CA 93943-5000		8. PERFORMING ORGANIZATION REPORT NUMBER		
9. SPONSORING/MONITORING AGENCY NAME(S) AND ADDRESS(ES)		10. SPONSORING/MONITORING AGENCY REPORT NUMBER		
11. SUPPLEMENTARY NOTES The views expressed in this thesis are those of the author and do not reflect the official policy or position of the Department of Defense or the U.S. Government.				
12a. DISTRIBUTION/AVAILABILITY STATEMENT Approved for public release; distribution is unlimited.			12b. DISTRIBUTION CODE	
13. ABSTRACT (maximum 200 words) This thesis documents experiments conducted with the Gsanger LM0202P electro-optic modulator to achieve a high percentage modulation at 125MHz of an argon-ion laser. The laser was tuned to produce a single mode, linearly polarized light at 514.5 nm. The laser light was first passed through the electro-optic crystal modulator with no external electric field applied, and the frequency spectrum was observed to be the same as the frequency spectrum of the source laser. When an AC voltage with a frequency of 125 MHz was applied to the modulator sidebands were observed by using a Fabry-Perot interferometer. Further measurements were taken to determine the suitability of the LM0202P modulator over a large frequency range.				
14. SUBJECT TERMS: High Frequency, Electro-Optic, Laser Modulation			15. NUMBER OF PAGES 54	
			16. PRICE CODE	
17. SECURITY CLASSIFICATION OF REPORT Unclassified	18. SECURITY CLASSIFICATION OF THIS PAGE Unclassified	19. SECURITY CLASSIFICATION OF ABSTRACT Unclassified	20. LIMITATION OF ABSTRACT UL	

NSN 7540-01-280-5500

Standard Form 298 (Rev. 2-89)  
Prescribed by ANSI Std. Z39-18 298-102



Approved for public release; distribution is unlimited.

**HIGH FREQUENCY CHARACTERIZATION OF THE GSANGER  
LM0202P ELETRO-OPTIC MODULATOR**

John R. Tucker  
Lieutenant, United States Navy  
B.S., United States Naval Academy, 1989

Submitted in partial fulfillment  
of the requirements for the degree of

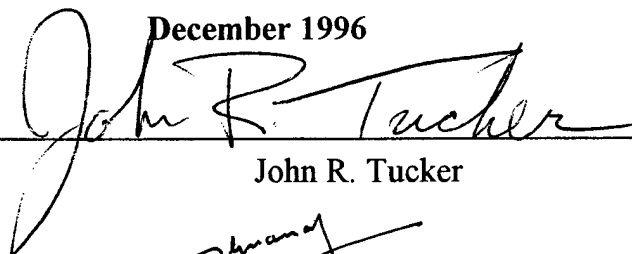
**MASTER OF SCIENCE IN APPLIED PHYSICS**

from the

**NAVAL POSTGRADUATE SCHOOL**

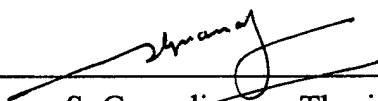
December 1996

Author:

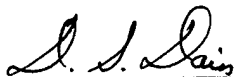


John R. Tucker

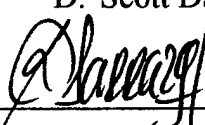
Approved by:



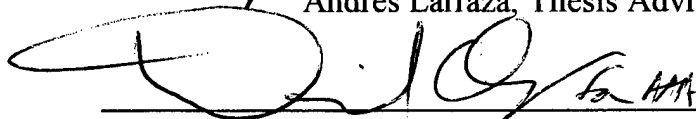
S. Gnanalingam, Thesis Advisor



D. Scott Davis, Thesis Advisor



Andrés Larraza, Thesis Advisor



Anthony A. Atchley, Chairman  
Department of Physics

**DTIC QUALITY INSPECTED 3**



## **ABSTRACT**

This thesis documents experiments conducted with the Gsanger LM0202P electro-optic modulator to achieve a high percentage modulation at 125MHz of an argon-ion laser. The laser was tuned to produce a single mode, linearly polarized light at 514.5 nm. The laser light was first passed through the electro-optic crystal modulator with no external electric field applied, and the frequency spectrum was observed to be the same as the frequency spectrum of the source laser. When an AC voltage with a frequency of 125 MHz was applied to the modulator sidebands were observed by using a Fabry-Perot interferometer. Further measurements were taken to determine the suitability of the LM0202P modulator over a large frequency range.



## TABLE OF CONTENTS

I. INTRODUCTION.....	1
II. ELECTRO-OPTIC MODULATION.....	3
A. ELECTRO-OPTIC MODULATION.....	3
1. Birefringence.....	3
2. Electro-Optic Crystals and Modulation.....	4
B. INTERFEROMETRIC SPECTROSCOPY.....	13
III. EXPERIMENTAL ARRANGEMENT.....	17
A. THE MODULATOR.....	17
B. THE LASER.....	19
C. THE MODULATOR MOUNT.....	20
D. THE HYBRID CIRCUIT.....	22
E. THE INTERFEROMETER.....	23
F. DRIVING AND DETECTIONS SYSTEMS.....	24
IV. OBSERVATIONS AND MEASUREMENTS.....	29
A. THE DC CURVE.....	29
B. OBTAINING THE SPECTRUM OF THE MODULATED LASER BEAM .....	34
V. CONCLUSIONS AND RECOMMENDATIONS.....	41
LIST OF REFERENCES.....	43
INITIAL DISTRIBUTION LIST.....	45

## I. INTRODUCTION

Imagine a beam of intense green light guided by an optical fiber. If the light is made to alternate in intensity at the source, theory predicts (Larraza, 1996) that there will be periodic locations down the fiber where you will see light alternating between red and blue. Moving further along, you will again see green light alternating in intensity. Providing that the fiber is long, and that there are minimal energy losses along the fiber, this pattern of behavior will continue indefinitely. This mechanism thus allows the possibility of providing tunable coherent light from a single-frequency source.

This "AM-FM conversion" effect (so named because of the way in which the wave alternates between amplitude and frequency modulation) should occur only when a wave interacts with itself. Such interaction is normally negligible, unless the electromagnetic field amplitude is sufficiently high. AM-FM conversion is thus an example of a nonlinear effect.

A possible application of the AM-FM conversion is to broadband tunable lasers using fiber optics (Larraza, 1996). An essential aspect of the proposed tunable laser is the mechanism for modulating the intensity of light of a monochromatic source. Electro-optic modulators are one of the different ways to modulate the intensity of a source.

This thesis project attempts to build on research conducted previously at the Naval Postgraduate School by Ladner (1996) and Wallace (1996) regarding the characteristic behavior of the Gsanger Opto-Elektronics LM 0202 P electro-

optic modulator. We evaluate its performance as an amplitude modulator of an argon ion laser beam at modulation frequencies in the range of 125 MHz.

The thesis is organized into five chapters. In Chapter II, we give a general background of the theory of electro-optic modulators and of Fabry-Perot spectroscopy. In Chapter III we describe the experimental arrangement. In Chapter IV, we provide the details of the measurements. In Chapter V, we present our conclusions and recommendations for future work.

## II. ELECTRO-OPTIC MODULATION

In this chapter we present the theory for electro-optic modulators, following closely the treatment by Karim (1990). Because the output of the modulator is analyzed by a Fabry-Perot interferometer, we also provide an overview of the basic principles of that type of interferometric spectroscopy.

### A. ELECTRO-OPTIC MODULATION

#### 1. Birefringence

Light propagates through a transparent crystal by exciting the electrons that bind the atoms or molecules which form the crystal. The electrons are driven by the E-field of the electromagnetic wave, and they re-radiate secondary wavelets which recombine, producing a resultant wave which moves on. The speed of the wave, and therefore the index of refraction, is determined by the frequency of the E-field and the responses of the inter-atomic or inter-molecular bonds to periodic stimulation. If the intermolecular binding forces of the crystal are anisotropic, the indices of refraction along the three principal axes of the crystal will manifest this anisotropy. Each principal axis will have a different index of refraction.

To illustrate this idea, consider a mass suspended in a box by three sets of paired springs. Each pair is oriented along one of three mutually orthogonal axes. Each set has a different spring constant. Therefore the characteristic resonant frequency along each axis is different. Now imagine that the mass-

spring system represents an atom or a molecule in a crystalline solid. If the E-field of a linearly polarized electromagnetic wave propagating through the crystal were parallel to the stiffest springs, analogous to the direction of strongest bonding, the natural resonant frequency of the bond would be relatively high, as compared to the other directions. Similarly, if the E-field were parallel to the direction of weakest bonding, the characteristic frequency would be lower. This implies that the behavior of a given source of monochromatic, linearly polarized light propagating through the crystal would be determined by the orientation of the principal axes of the crystal relative to the orientation of the plane of polarization of the light. That is, the index of refraction along each axis is different, and the light with different polarizations moves through the crystal at different speeds. This property is known as birefringence.

## **2. Electro-optic crystals and modulation**

In the case of uniaxial crystals, the kind used for electro-optic modulation, one of the principal axes coincides with the axis of symmetry of the crystal. In this case, there are only two indexes of refraction. Taking the xy- plane as a plane of symmetry of the crystal, and the z-axis as the symmetry axis, the propagation of light along this axis will be characterized by the ordinary index of refraction  $n_o$ . Propagation of light along the xy- plane will be characterized by the extraordinary index of refraction  $n_e$ . For an arbitrary orientation of the direction of propagation an incident beam of light can be decomposed into two orthogonally polarized components. One component moves with a speed

determined by  $n_o$  and the other component moves with a velocity determined by  $n_e$ . This can cause the double image characteristic exhibited by some birefringent crystals.

For a uniaxial crystal, if the linearly polarized light wave propagates along the z-axis, the index of refraction will be  $n_o$ . Rotating the crystal about the z-axis will not change the observed index of refraction. However, if the light is propagating along the x-axis, rotating the crystal will vary the observed index of refraction between  $n_o$  and  $n_e$ .

For some crystals an external electric field can alter the index of refraction and hence the propagation speed. Consider the propagation of light in such a crystal in the absence of an externally applied electric field. The refractive indices along the respective rectangular coordinate axes of the crystal are related by an index ellipsoid described by

$$\left(\frac{x}{n_x}\right)^2 + \left(\frac{y}{n_y}\right)^2 + \left(\frac{z}{n_z}\right)^2 = 1 \quad . \quad (2.1)$$

However, if we apply an external electric field, a change in optical symmetry may occur, and here the effect may be of the first order in the field. This linear effect will induce a change in the coefficients of the index ellipsoid which can be represented by

$$\Delta\left(\frac{1}{n^2}\right)_i = \sum_j p_{ij} E_j \quad (2.2)$$

This is known as the Pockels effect. The  $p_{ij}$  are the Pockels constants,  $i = 1, 2, 3, 4, 5, 6$ ; and  $j = x, y, z$ . The  $6 \times 3$  electro-optic matrix is known as the electro-optic tensor which is a tensor of rank three,  $p_{ikj}$ , symmetrical in the suffixes  $i$  and  $k$  ( $p_{ikj} = p_{kij}$ ). When representing the electro-optic tensor in matrix form, the indices  $i$  and  $k$ , which take on values 1, 2, 3, are contracted into single index  $i$  with the correspondence  $1=(11)$ ,  $2=(22)$ ,  $3=(33)$ ,  $4=(23)=(32)$ ,  $5=(13)=(31)$ ,  $6=(12)=(21)$ . The new index ellipsoid is obtained by adding to Eq. (2.1) the tensor contraction of Eq. (2.2) with the tensor dyadic form from the three principal directions of the crystal.

Determining the electro-optic effect in the modulator involves using the characteristics of the crystal and finding the principal polarization directions for a given propagation direction. Knowledge of the refractive indices along the principal directions can be used to decompose the incident optical wave along those principal polarization directions. We can then predict the characteristics of the emergent optical wave.

Consider the case of an optical wave propagating through a crystal of potassium dihydrogen phosphate ( $\text{KH}_2\text{PO}_4$ ) or KDP. In this case the only nonzero Pockels constants are  $p_{41}=p_{52}$ , and  $p_{63}$ . In the presence of an external field, the index ellipsoid is described by

$$\frac{x^2 + y^2}{n_o^2} + \left(\frac{z}{n_e}\right)^2 + 2p_{41}yzE_x + 2p_{41}xzE_y + 2p_{63}xyE_z = 1 \quad , \quad (2.3)$$

with  $n_x=n_y=n_o$ , and  $n_z=n_e$ . If the field is applied along the z-direction, Eq. (2.3)

reduces to

$$\frac{x^2 + y^2}{n_o^2} + \left(\frac{z}{n_e}\right)^2 + 2p_{63}xyE_z = 1 \quad . \quad (2.4)$$

We can transform equation (2.4) to a form of the type

$$\left(\frac{x'}{n_{x'}}\right)^2 + \left(\frac{y'}{n_{y'}}\right)^2 + \left(\frac{z'}{n_{z'}}\right)^2 = 1 \quad , \quad (2.5)$$

which has no mixed terms. The parameters  $x'$ ,  $y'$ , and  $z'$  denote the directions of major axes of the index ellipsoid in the presence of the external field. The lengths of the major axes of the index ellipsoid are given by  $2n_x$ ,  $2n_y$ , and  $2n_z$ , respectively.

By comparing equations (2.4) and (2.5) we find that  $z$  and  $z'$  are parallel to each other. The symmetry in Eq (2.4) to an exchange in  $x$  and  $y$  suggests that  $x'$  and  $y'$  are related to  $x$  and  $y$  by a rotation of 45 degrees. Thus

$$\left[\frac{1}{n_o^2} + p_{63}E_z\right]x'^2 + \left[\frac{1}{n_o^2} - p_{63}E_z\right]y'^2 + \left(\frac{z'}{n_e}\right)^2 = 1 \quad . \quad (2.6)$$

Comparing equations (2.5) and (2.6) and using the differential relation  $dn = - (1/2)n^3 d(1/n^2)$ , we find that,

$$n_{x'} = n_0 - \frac{1}{2}n_0^3 p_{63} E_z \quad , \quad (2.7a)$$

$$n_{y'} = n_0 + \frac{1}{2}n_0^3 p_{63} E_z \quad , \quad (2.7b)$$

$$n_{z'} = n_e \quad , \quad (2.7c)$$

when  $1/n_0^2 \gg p_{63} E_z$ . The velocity of propagation of an emerging wave polarized along the  $x'$ -axis differs from that of the emerging wave polarized along the  $y'$ -axis.

In a transverse electro-optic modulator, such as the one we characterize in this thesis, the crystal is oriented such that the polarization vector of the incident beam lies in the  $x'z$ -plane at  $45^\circ$  degrees from the  $x'$ -axis, while the light propagates along the  $y'$ -axis and an external field is applied by parallel plate electrodes mounted normal to the  $z$ -axis. The velocity of propagation of an emerging wave polarized along the  $x'$ -axis differs from that of an emerging wave polarized along the  $z$ -axis. The corresponding phase shift difference between the two waves (referred to as electro-optic retardation) after having traversed a crystal of length  $L$  and width  $d$  is given by

$$\Gamma = \frac{(2\pi)L}{\lambda_0} \left[ (n_o - n_e) - n_o^3 p_{63} \frac{V}{d} \right] \quad (2.8)$$

The value of  $V$  for which  $\Gamma = \pi$  is called the half-wave voltage,  $V_\pi$ . For a transverse electro-optic modulator, long crystals with small width have a low half-wave voltage. Similarly, propagation along the crystal axis with the parallel plate electrodes mounted normal to the  $z$ -axis corresponds to a longitudinal electro-optic modulator. In this case the relative retardation is independent of the length and the width of the crystal and the half-wave voltage may be significantly higher.

This electrically induced birefringence can cause a light wave traveling along the  $y$ -axis of a crystal of length  $L$ , with its polarization initially parallel to the  $x$ -axis, to acquire a polarization parallel to the  $z$ -axis. The  $z$ -component of polarization grows at the expense of the  $x$ -component as the total polarization of the traveling wave cycles through elliptical polarization, then circular polarization, then elliptical polarization again, until the plane of polarization has rotated 90 degrees (Figure 2.1).

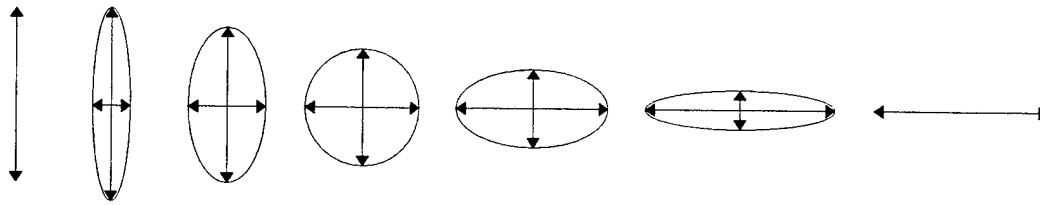


**Figure 2.1** As the vertically polarized light wave propagates through the electro-optic crystal the plane of polarization is rotated 90 degrees

If one were to place a polarizer at the output plane of the crystal that is perpendicular to the initial plane of polarization of the incident wave, the optical beam would be completely attenuated when the electric field is off. But when the field is applied, the perpendicular component of polarization would increase in proportion to the applied voltage. At the half-wave voltage  $V_{\pi}$ , the polarization is rotated 90 degrees and the light exiting the crystal would pass unattenuated by the polarizer. By varying the applied electric field the flow of optical energy can be controlled. This serves as the basis of the electro-optic amplitude modulation of light.

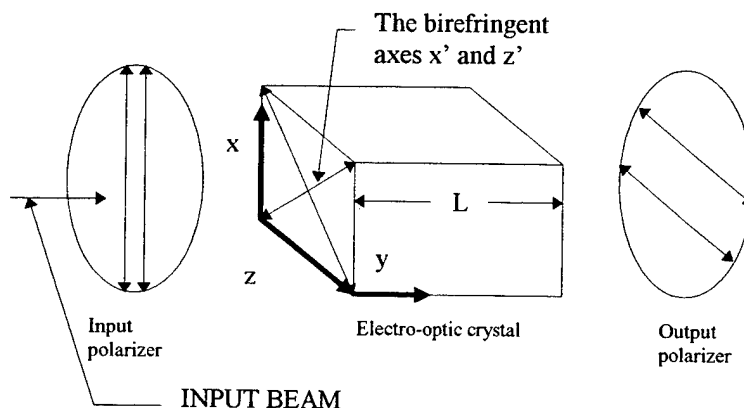


**Figure 2.2** A typical arrangement of an electro-optic modulator.

Consider the arrangement in Figure 2.2, which consists of an electro-optic crystal bounded at either end by crossed polarizers, which in turn are at an angle of 45 degrees with respect to the electrically induced birefringent axes  $x'$  and  $z'$ . The optical wave reaches the input face of the crystal with a vertical polarization, parallel to the  $x$ -axis. Thus it has equal in-phase components along  $x'$  and  $z'$  which we take as,

$$\begin{aligned} e_{x'} &= A \cos \omega t \\ e_{z'} &= A \cos \omega t \end{aligned} \quad (2.9)$$

Using the complex amplitude notation,

$$\begin{aligned} E_{x'}(0) &= A \\ E_{z'}(0) &= A \end{aligned} \quad (2.10)$$

The incident intensity is thus,

$$I_i = |E_{x'}(0)|^2 + |E_{z'}(0)|^2 = 2A^2 \quad (2.11)$$

When the optical wave exits the crystal the  $x'$  and  $z'$  components have acquired a relative phase shift of  $\Gamma$  radians. We may take them as

$$\begin{aligned} E_{x'}(L) &= Ae^{-i\Gamma} \\ E_{z'}(L) &= A \end{aligned} \quad (2.12)$$

The total complex field emerging from the output polarizer is the sum of  $E_{x'}(L)$  and  $E_{z'}(L)$  along the analyzer, which gives

$$E_o = \frac{A}{\sqrt{2}}(e^{-i\Gamma} - 1) \quad (2.13)$$

This corresponds to an output intensity of

$$I_o = \frac{A^2}{2} [(e^{-i\Gamma} - 1)(e^{i\Gamma} - 1)] = 2A^2 \sin^2 \frac{\Gamma}{2} \quad (2.14)$$

The ratio of the output intensity to the input intensity is thus

$$\frac{I_o}{I_i} = \sin^2 \frac{\Gamma}{2} = \sin^2 \left[ \left( \frac{\pi}{2} \right) \frac{V}{V_\pi} \right] \quad (2.15)$$

Thus in Eq. (2.15), zero applied voltage corresponds to total extinction in the electro-optic modulator. As the applied voltage increases to the half-wave voltage, the transmission (output) intensity increases to 100 percent. By applying a sinusoidal modulating voltage about the 50% output intensity voltage,

$\frac{1}{2}V_{\pi}$ , a sinusoidal modulation of the optical beam can be induced. This can be represented mathematically by writing

$$V = \frac{1}{2}V_{\pi} + V_p \sin \omega_m t \quad (2.16)$$

For peak voltages smaller than  $\frac{1}{2}V_{\pi}$ , the intensity modulation is a linear replica of the modulating voltage. On the other hand, if the modulating voltage is comparable to  $\frac{1}{2}V_{\pi}$ , it follows from Eq (2.15) that the intensity variation is distorted and will contain an appreciable amount of odd harmonics of the fundamental modulation frequency.

## **B. INTERFEROMETRIC SPECTROSCOPY**

A Tropel 350 Fabry-Perot interferometer was used to analyze the frequency spectrum of the laser beam in this experiment. It consists of two parallel glass surfaces, coated with a highly reflecting dielectric film. The parallel surfaces are separated by a distance  $d$ . One plate is mounted on three differential micrometer assemblies to allow for fine adjustment of parallelism. When these two surfaces are held adjusted for parallelism they are referred to as an etalon. The other plate is attached to an electrically driven motor and moves back and forth a distance of the order of one wavelength (Fig 2.3). A portion of the laser beam entering the interferometer through one of the plates is multiply reflected between the two plates. If the etalon is aligned properly, this will set up a standing wave which will cause constructive interference at the

output of the interferometer, and produce a circular interference pattern consisting of light and dark fringes. Each half wavelength of plate travel produces a phase shift of  $2\pi$ , corresponding to one order of constructive interference. The separation in frequency between successive spectral orders is called the free spectral range (FSR) and is related to the etalon spacing by

$$\text{FSR} = \frac{c}{2nd} \quad , \quad (2.17)$$

where  $c$  and  $n$  are the speed of light and index of refraction of the inter-plate medium and  $d$  is the inter-plate spacing. In this case the medium is air, so  $n \approx 1$ . By changing the plate separation  $d$ , we change the FSR, and this allows us to adjust the resolving power as required. The goal of this research was to observe 125MHz modulation of the laser with an electro-optic modulator. The high resolving power of the Fabry-Perot interferometer provides the means to observe the modulation sidebands, and to determine the effect that the modulation is having on the laser beam light.

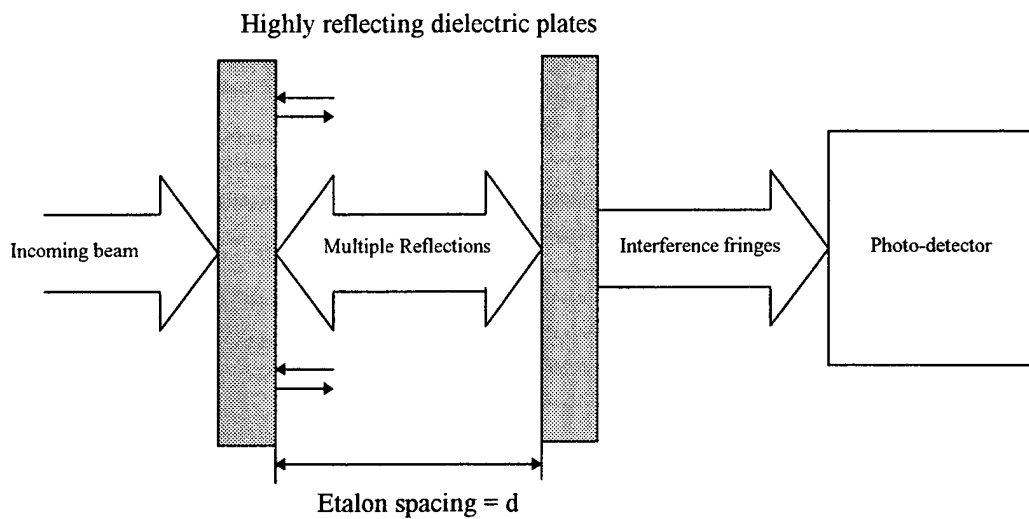


**Figure 2.3** Fabry-Perot interferometer uses glass plates coated with a highly reflecting dielectric film. The beam enters and a portion of it is reflected back and forth between the two etalons, one of which is moving the distance of about one wavelength. This causes constructive and destructive interference producing an interference pattern on the photo-detector.



### III. EXPERIMENTAL ARRANGEMENT

In this chapter we provide a description of the components used in our experiment. Figure 3.1 shows the schematic of the experimental arrangement.

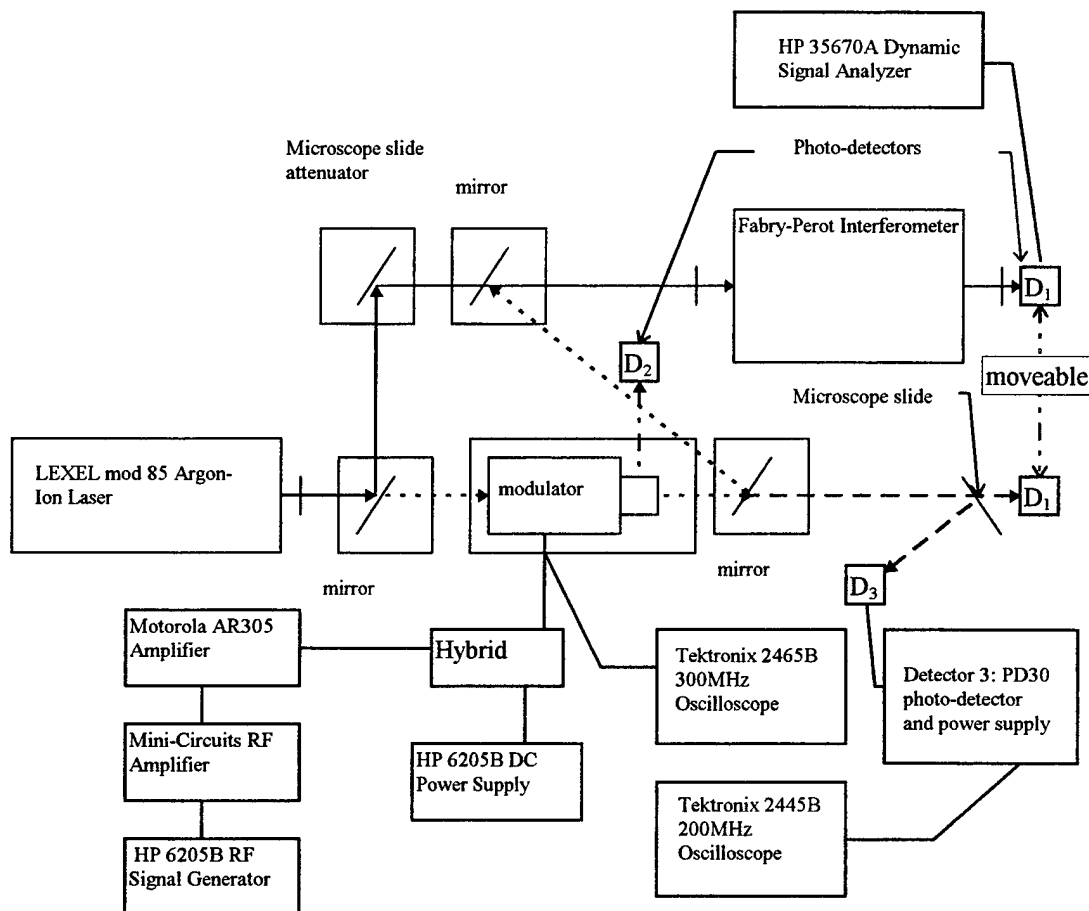


**Figure 3.1.** The modulator, the mirrors, and microscope slides were supported by kinematic mounts, allowing the beam path to be changed quickly. Detector 1 (D<sub>1</sub>) was alternated between the two positions indicated as required by the experiment.

#### A. THE MODULATOR

The Gsanger Opto-Elektronics Model LM0202P electro-optic modulator (Fig 3.2) is the principal component of this experimental investigation. The

modulator was designed to function as a Pockels cell. The laser light passing through the cell can be amplitude modulated by applying a varying voltage to the birefringent crystals in the cell. According to the manufacturer, the LM0202P electro-optic modulator is designed to modulate a laser beam with an intensity of 0.1 to 5 Watts at modulation frequencies up to 150 MHz. In our experiment the beam intensity was in the range of 75-100 mW and our goal was to achieve 100% modulation at 125MHz.

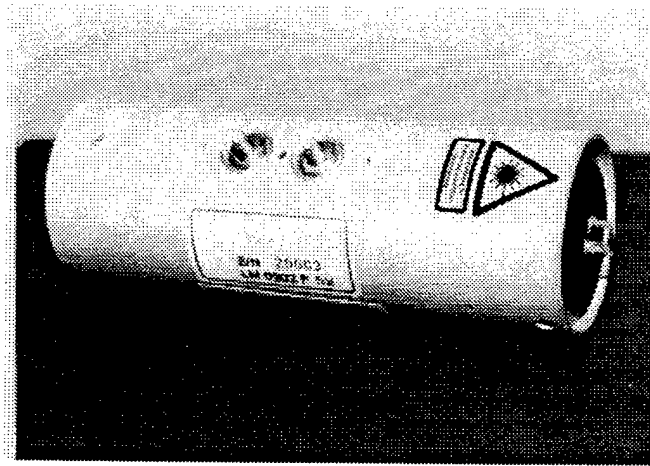


**Figure 3.2.** The LM0202P transverse electro-optic modulator. Shown in the picture are the Brewster cube mounted at the exit end and the microdot connectors on the side. The input aperture is a 3×3 mm square.

As stated in Chapter II, the LM0202P is a transverse electro-optic modulator, with four electro-optic crystals operating in series. As the beam passes through each crystal its polarization mode changes. At the downstream end of the modulator there is a Brewster cube that splits the laser beam into its two mutually orthogonal polarized components. As depicted in Figure 3.3, the horizontally polarized component passes straight through the modulator, while

the vertically polarized component is deflected 90 degrees. With no applied voltage, the horizontally polarized component is extinguished, while at the half-wave voltage the vertically polarized component is extinguished.

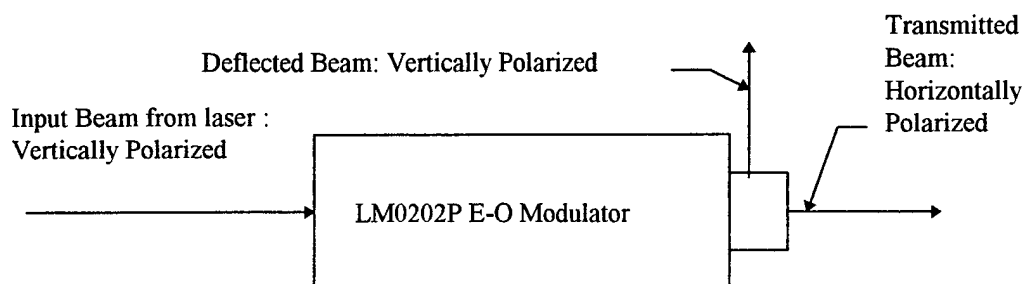


**Figure 3.3.** Schematic of the modulator. With no applied voltage, the transmitted (horizontally polarized) beam is extinguished. When the applied voltage equals the half-wave voltage, the deflected (vertically polarized) beam is extinguished.

## B. THE LASER

The laser was supported at one end of the optical bench on two standard lab jacks. It was tuned to optimal single mode operation by adjusting the two knobs labeled HORIZONTAL and VERTICAL & WAVELENGTH located at the rear end of the laser. The laser must be operating in the current-control mode whenever tuning is performed. The knobs are used alternately in an iterative process in order to obtain the desired wavelength and intensity. The VERTICAL & WAVELENGTH knob selects the wavelength by adjusting an etalon within the laser resonant cavity. A counterclockwise turn selects a longer wavelength and a clockwise turn selects a shorter wavelength. The peak power is adjusted after each wavelength change by using the HORIZONTAL tuning knob and adjusting for peak output power.

The laser frequency spectrum was measured with a Fabry-Perot interferometer along with the dynamic signal analyzer. The laser was adjusted to optimize single mode output by observing the spectrum. The spectrum was viewed on the HP 35670A digital signal analyzer. A pinhole aperture, made by poking a small hole (estimated diameter  $\cong$  100 microns) through a piece of aluminum foil, was positioned in the beam path directly in front of D1. This aperture, in conjunction with the other optics, functioned as a spatial filter to minimize the field of view of the detector.

### **C. THE MODULATOR MOUNT**

An effective means for mounting the modulator, shown in Figure 3.4, was devised by using a micro-rotary positioner mounted on a New Focus 9082 tilting stage which allows five degrees of freedom: translation in the x, y, and z axis and limited rotation about the x and y axes (ie: tilting in pitch and yaw). The tilting stage was attached to a kinematic mount which allowed the modulator to be moved in and out of the beam path without requiring readjustment. The modulator was fitted into the micro-rotary positioner by means of a home made aluminum adapter.

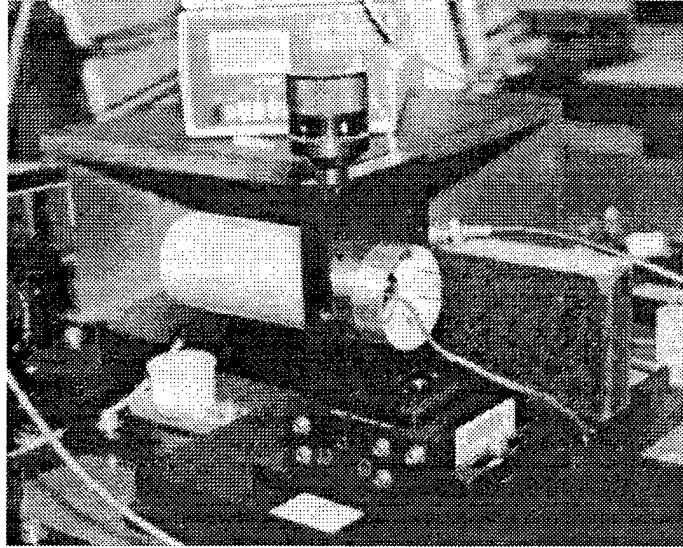


**Figure 3.4.** Modulator mounted on the azimuthal and tilting stages.

This mount allowed micro-rotary adjustment of the modulator in the azimuthal direction to micro-radian tolerances. It also positioned the entry window of the modulator over the center of rotation of the tilting stage. Finally, the metal mount exposed more surface area of the cell to the air to allow for greater passive cooling in order to minimize possible drifts due to thermal variations in the modulator.

By positioning the LM0202P modulator in the beam path with the analyzer down beam from the window end, and with the beam centered on the entry window, the modulator was tilted so the reflection off the window coincided with the input beam. This was achieved by mounting a two inch aluminum disk between the laser and the modulator. A two millimeter hole drilled through the center of the disk allowed the beam through the aperture. The position of the reflection from the window could be viewed relative to the beam by observing the

reflection on the aluminum disk. However, the reflection from the window was asymmetrical which made this adjustment more art than science. Nevertheless, this procedure yielded reliable and reproducible results. The modulator was then rotated about its longitudinal axis so the intensity of the horizontally polarized transmitted beam was minimized while the intensity of the vertically polarized reflected beam was maximized. This step ensured that the x and z axes were properly positioned with respect to the incident laser beam, which was vertically polarized.

#### **D. THE HYBRID CIRCUIT**

When an AC voltage is applied, the electro-optical crystal heats up, because the dipoles in the crystal are oscillating back and forth. As the frequency of the modulation increases from kilohertz to megahertz, this effect becomes more pronounced. This thermal effect may modify the indices of refraction of the birefringent crystals. Therefore when conducting the experiment the modulator needed about 3-5 minutes to stabilize at a new thermal equilibrium whenever the modulation signal was changed. A compensating DC bias voltage was then applied in order to keep the modulator centered at the crossover point as is discussed in Chapter IV. A hybrid circuit, as depicted in Fig. 3.5, was used to allow for the DC biasing of the modulator while the RF signal was applied simultaneously.

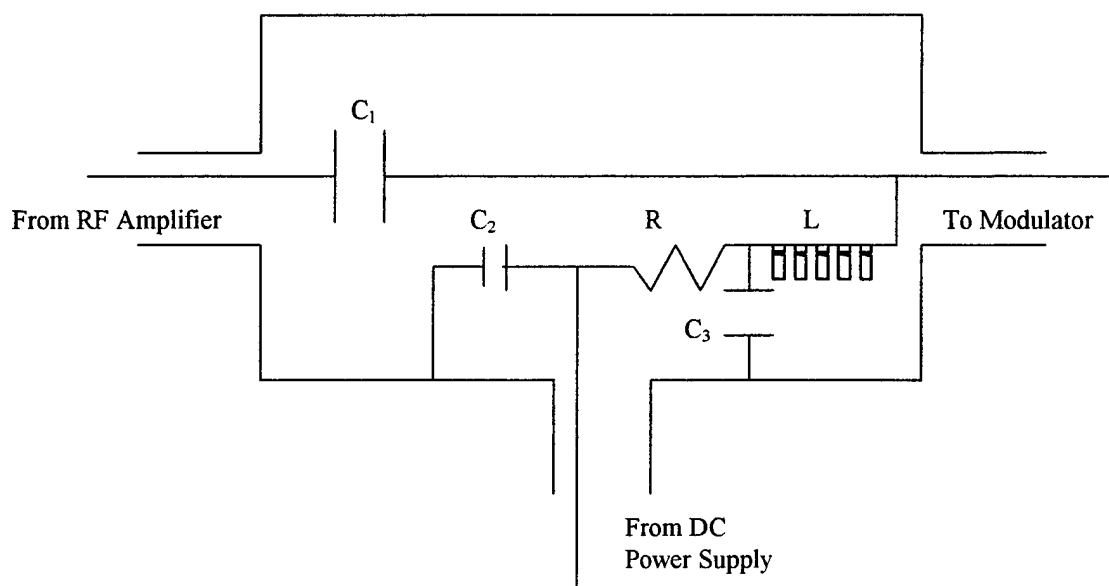


**Figure 3.5.** The Hybrid Circuit:  $C_1 = 0.01\mu\text{F}$ ,  $C_2 = C_3 = 0.0047\mu\text{F}$ ,  $R = 100\text{k}\Omega$ ,  $L = \text{RF choke } 1\mu\text{H}$ .

## E. THE INTERFEROMETER

The Fabry-Perot interferometer as described in Chapter II, dictated the physical arrangement of the overall experiment. The device was extremely sensitive to the most minute adjustments, and it was absolutely crucial to have the beam traverse the center of the etalon perpendicularly to the plate surfaces. The interferometer's optical axis was the geometric reference around which the rest of the experiment was aligned. Once it was properly adjusted, it was held fixed.

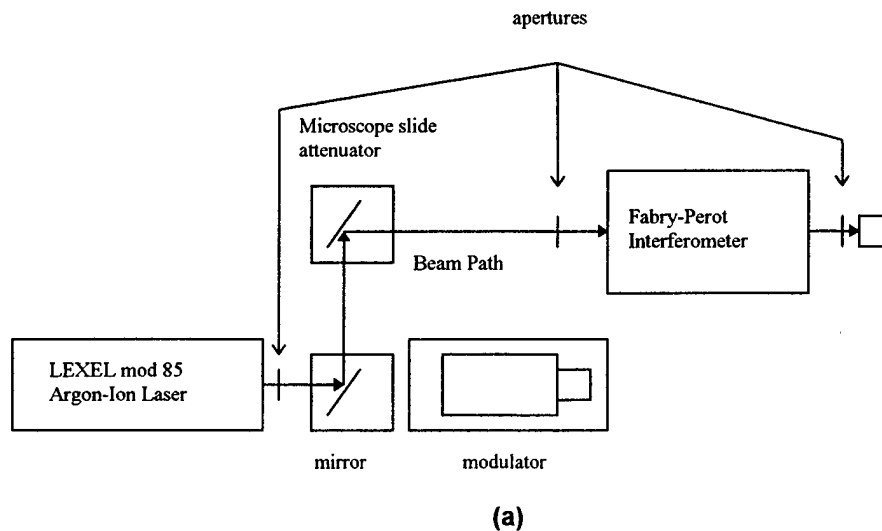
## **F. DETECTION AND DRIVING SYSTEMS**

The photo-detectors used in the experiment were of two types. The two Newport 818 SL photo-detectors, each connected to its own Newport 815 Series power meter, were primarily used to measure the transmitted and deflected beam intensities. They are identified respectively as detector 1 (D1) and detector 2 (D2) in this thesis. They both converted the power of the incident light to a DC voltage signal. D1 was also used at the output of the Fabry-Perot interferometer to record the fringes. The voltage signal was then routed to the HP 35670A dynamic signal analyzer which monitored and recorded the data. D1 and D2 are however, limited in frequency response to only 180 kHz and would not be useful in detecting the 125 MHz modulation of the laser beam.

An Opto-Electronics PD30 photo-detector, identified as detector 3 (D3), was used to detect modulation in the transmitted beam because it had a specified bandwidth of 1GHz. However, the PD30 photo-detector saturates at an optical power of 3mW, though it was required to monitor a beam intensity that varied from 0-60mW. A microscope slide was used to reflect a fraction of the beam onto D3 (Fig 3.1). This microscope slide attenuated the optical power and provided the additional benefit of making it possible to simultaneously monitor the transmitted beam intensity with D1, which was mounted directly in the main beam path behind the microscope slide. Detector 1 was calibrated to account for the 10% of the beam intensity being reflected into detector 3.

Due to the large number of electronic and optical devices used in the experiment, bench space was limited. The modulator, the laser and the

interferometer were all very sensitive to small perturbations and difficult to realign quickly. Efficiency dictated that, once they had been aligned and adjusted, they were not to be disturbed. In order to optimize the use of bench space and to minimize the time required to transition between optical configurations, two different beam paths were used. Mirrors and microscope slides were attached to kinematic mounts which allowed for their rearrangement, without requiring constant readjustment. Each beam path had its own set of reflectors. One beam path went around the modulator so a spectrum of the direct unmodulated laser light could be measured (Fig 3.6.a). The other beam path was routed through the modulator so the AM spectrum could be measured (Fig 3.6.b).



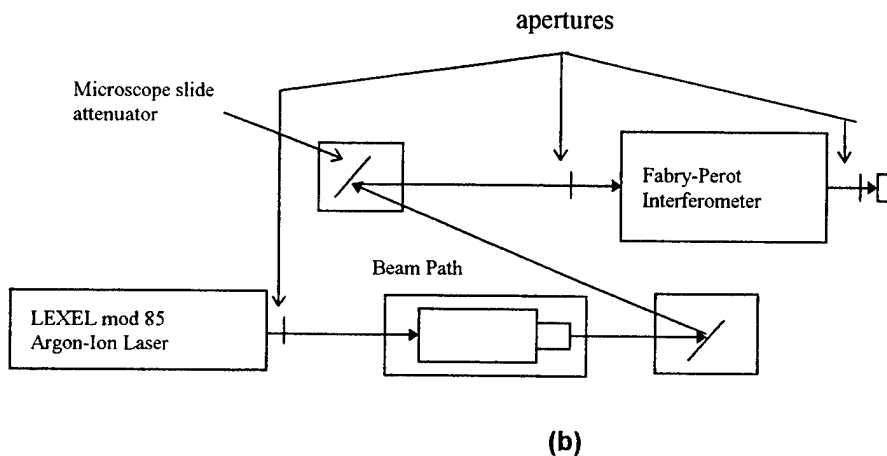


**Figure 3.6. (a)** Beam path for baseline measurements. **(b)** Beam path through modulator.

For both the baseline measurements of the laser beam (Fig 3.6.a) and the beam coming out of the modulator (Fig 3.6b), a microscope slide attenuator was used to reduce the optical power into the interferometer. The back side of the microscope slide was scratched with sandpaper to defuse the light reflecting off the back surface, thus minimizing interference caused by the secondary reflection.

Two oscilloscopes, a Tektronix 2445B (200 MHz) and a Tektronix 2465 (300 MHz), were used to monitor the applied electrical signal and the resultant modulation. The reason for using two separate oscilloscopes was that internal coupling between channels, at very high frequencies interfered with the observed modulation signal when only one multi-channel oscilloscope was used. The applied electrical signal (20 -160  $V_{p-p}$ ) was several orders of magnitude greater than the modulation signal (mV) from the photo-detector, hence vastly different oscilloscope sensitivities were required.

An HP 8640B Signal Generator provided the RF signal for driving the modulator at 125 MHz. The output of the generator (maximum of  $3V_{rms}$ ), was amplified with a Mini-Circuits RF power amplifier providing signal amplification up to  $40 V_{p-p}$ . A second stage amplifier, a Motorola AR305 RF, was used for amplitudes above  $40 V_{p-p}$  up to  $160 V_{p-p}$ . The Motorola amplifier was powered by an HP 6274B DC power supply. An HP 6209B DC power supply provided the DC bias to the modulator.



## IV. OBSERVATIONS AND MEASUREMENTS

### A. THE DC CURVE

To determine the half-wave voltage of the modulator, we determined its DC characteristic response curve. The experimental arrangement used for that purpose is shown in Figure 4.1.

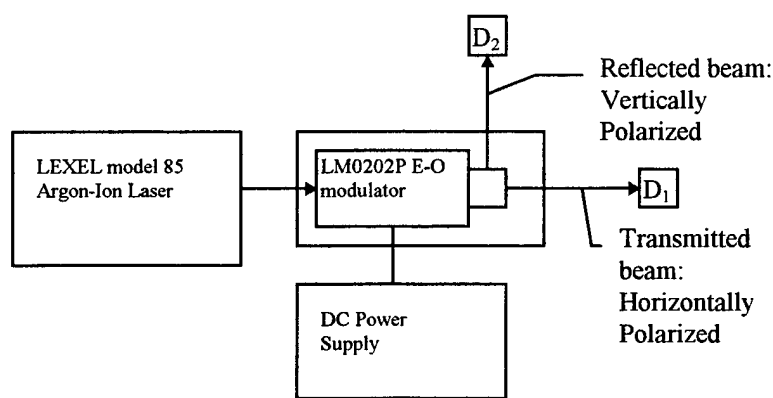


**Figure 4.1.** Arrangement for recording the DC characteristic curve.

The modulator was aligned for maximum extinction of the transmitted beam (horizontal polarization) as measured by detector D<sub>1</sub>, when the applied voltage was zero. The DC voltage was then increased from zero to 330 volts, in steps of 10 volts, and the readings of D<sub>1</sub> and D<sub>2</sub> were noted at each step. The results are plotted in Figure 4.2.

At the point where the two curves cross, the modulator behaves as a quarter-wave plate, and 50% of the beam is transmitted (horizontally polarized) while 50% is reflected (vertically polarized). This point will henceforth be referred to as the crossover point. Applying a sinusoidal electrical signal to the

modulator modulates the transmitted beam about the crossover point. Increasing the amplitude of the applied AC signal increases the percentage of modulation approximately linearly until the peak-to-peak amplitude of the applied electrical signal approaches the half-wave voltage of the modulator. This coincides with the maximum and minimum points on the characteristic curve. As the modulation of the transmitted beam reaches a maximum, the relationship between the amplitude of the applied AC signal and the percentage modulation of the beam is no longer linear. Over-modulation of the beam occurs if the half-wave voltage is exceeded.

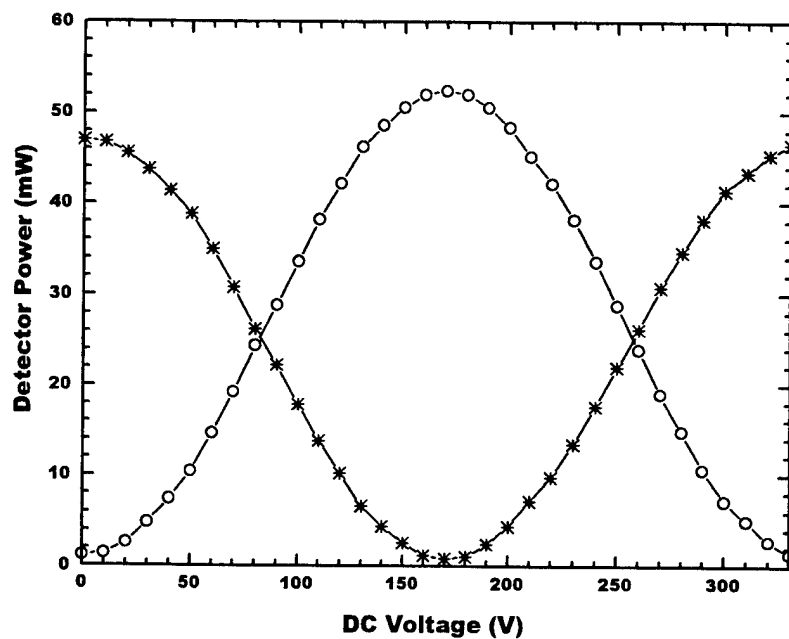


**Figure 4.2.** The DC characteristic curve for the LM0202P electro-optic modulator. The open diamonds correspond to the transmitted beam measured by D1 (horizontally polarized) and the stars correspond to the beam measured by D2 (vertically polarized).

On the basis of the DC characteristic of the modulator, it is expected that an applied AC voltage of 120 volts peak-to-peak would result in about a 90% modulation, with the modulator operating at the crossover point. However, when this AC voltage at 125 MHz was applied to the terminals of the modulator, the actual percentage modulation observed in the optical beam was only about 20%. This clearly confirmed the conclusion previously reached by Ladner (1996), that only a fraction of the RF voltage applied to the modulator terminals reached the electro-optic crystal. A large fraction of the applied signal was taken up by the large high frequency inductive reactance of the internal wire leads to the crystal. Furthermore, it was observed that the percentage modulation hardly increased when the applied 125MHz AC voltage was increased from 100 volts peak-to-peak to 140 volts peak-to-peak. A possible explanation for this behavior is that there was appreciable dielectric loss in the electro-optic crystal at very high-frequencies. The electrical behavior of the crystal is thus equivalent to that of a capacitance in parallel with a resistance, and the value of the resistance decreases steeply when the RF voltage across the crystal is increased. The equivalent circuit of the modulator is shown in Figure 4.3. Future experiments designed to specifically measure the electrical characteristics of the modulator will address this issue.

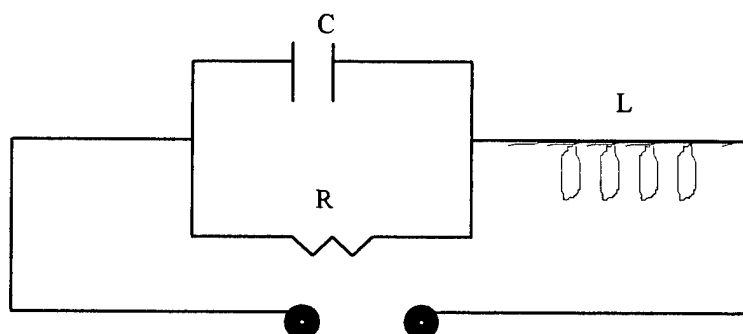


**Figure 4.3.** Equivalent circuit for the modulator. C is the capacitance of the crystal, R is the resistance equivalent to dielectric loss, L is the inductance of the wire leads inside the modulator.

Inspection of the DC characteristic curve, Figure 4.2, shows that the percentage modulation measured by  $D_1$  ( the intensity of the transmitted horizontally polarized beam) could be increased by lowering the mean value of the reading of  $D_1$  below the crossover point, while maintaining the AC excursion of the reading of  $D_1$  at a constant amplitude. We adopted this method, even though it would result in nonlinear modulation and a slightly distorted modulation envelope. It turned out that the percentage modulation could be increased from 20% to 80% at 125MHz without serious distortion, by suitably adjusting the DC voltage to lower the mean value of the reading of  $D_1$  while maintaining the AC voltage at 60 volts peak-to-peak.

A study of the modulator's DC characteristic reveals that when the mean value of the reading of  $D_1$  is made too small, the negative peaks of the modulation envelope become flattened, and the effective percentage modulation decreases. We performed measurements to determine the mean value of the reading of  $D_1$  that would yield the highest percentage modulation. Figure 4.4 shows the results of these measurements.

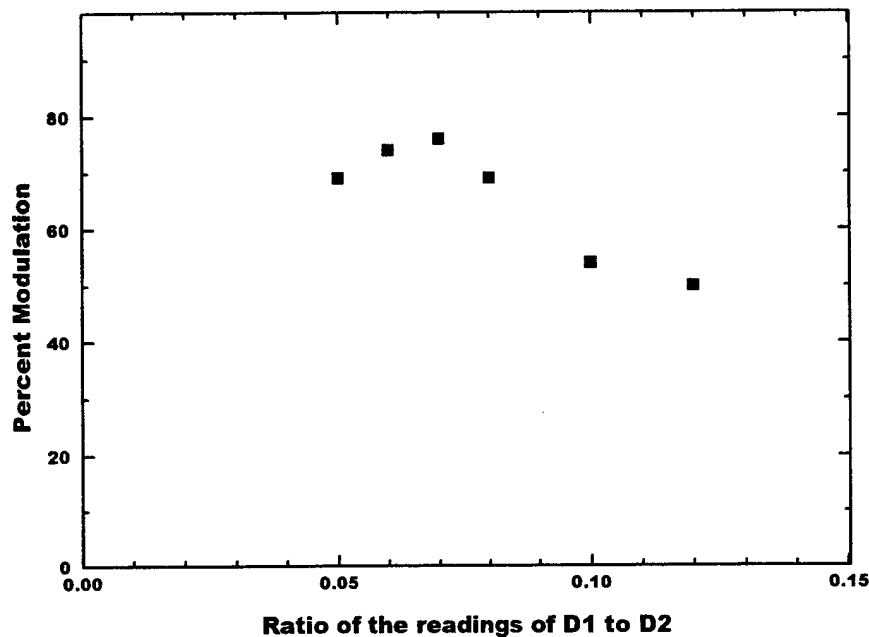


**Figure 4.4.** Percent Modulation vs ratio of the power output measured by detectors  $D_1$  and  $D_2$ . The percentage modulation obtained with an applied AC voltage of 60 volts peak-to-peak at 125 MHz is plotted against the ratio of the mean value of the reading of  $D_1$  to the mean value of the reading of  $D_2$ .

The percentage modulation obtained with an applied AC voltage of 60 volts peak-to-peak at 125 MHz is plotted against the ratio of the mean value of the reading of  $D_1$  to the mean value of the reading of  $D_2$ . A plot of percentage of modulation against the mean value of the reading of  $D_1$  would have yielded inconsistent results because the absolute values of the readings of  $D_1$  and  $D_2$  were subject to variability, depending upon the output of the laser and the percentage transmission of the modulator. The ratio of the readings of  $D_1$  over the readings of  $D_2$  that yielded the highest percentage modulation was 0.07.

We also performed experiments to determine the variation of the percentage modulation with the applied AC voltage at the crossover point and at

a low modulation frequency of 20 kHz, an intermediate frequency of 20 MHz, and a high frequency of 125 MHz. Figure 4.5 shows a comparison between the percentage modulation at these frequencies and the percentage modulation predicted from the DC characteristic. The deleterious effects of the inductance of the internal wire leads to the crystal, and the presumed high frequency dielectric loss in the crystal are both clearly evident.

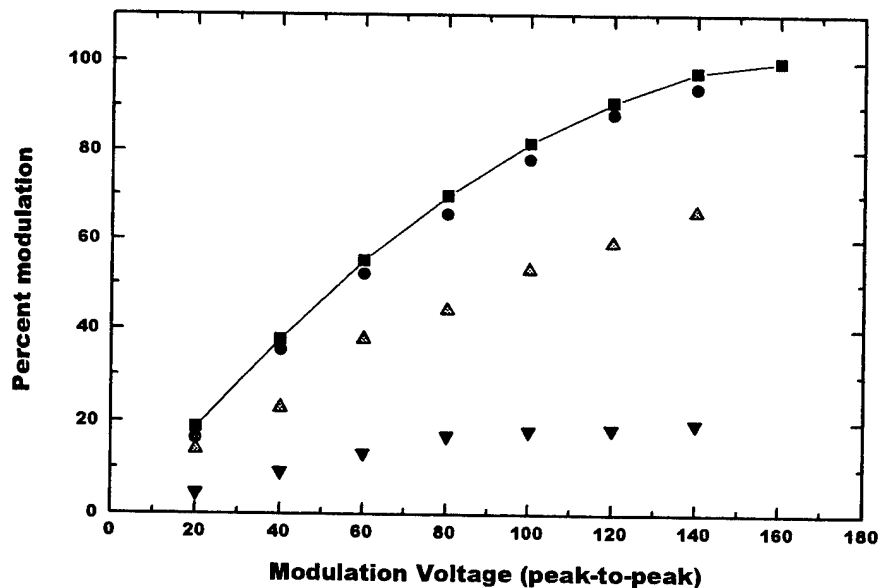


**Figure 4.5.** Percent modulation vs. modulation voltage for DC (solid squares), 20 kHz (solid circles), 20 MHz (up triangles), and 125 MHz (down triangles).

## B. OBTAINING THE SPECTRUM OF THE MODULATED LASER BEAM

During measurements of actual AM modulation, the laser intensity was held constant and all major components were mechanically fixed. Because of the sensitivity to alignment conditions, the process of taking measurements was organized to be done quickly in a consecutive sequence. The first step required

setting the beam path to route the beam around the modulator, so baseline measurements of the laser spectrum could be taken. Figure 4.6 shows the spectrum of the laser beam, before it enters the modulator. The etalon spacing was set to 10 cm, corresponding to a FSR of 1.5GHz.

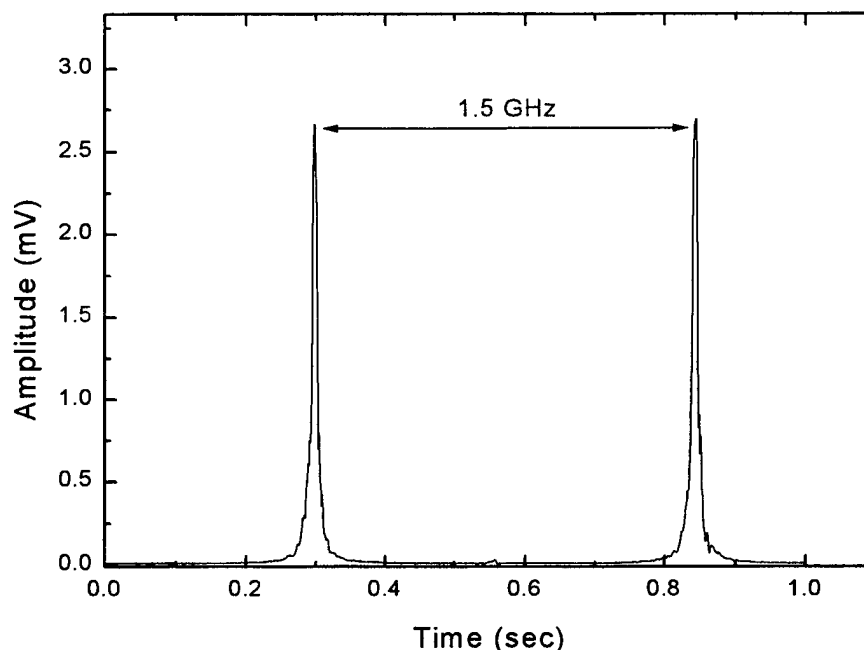


**Figure 4.6.** Baseline spectrum. The laser was tuned for single mode operation. The FSR is 1.5 GHz.

Immediately after obtaining the laser baseline spectrum, the beam was routed through the modulator with no voltage applied. Figure 4.7 shows the resulting spectrum. Comparing the Figures 4.6 and 4.7, indicates there is a reduction in light intensity in the modulator, but no extraneous structure is added to the spectrum.

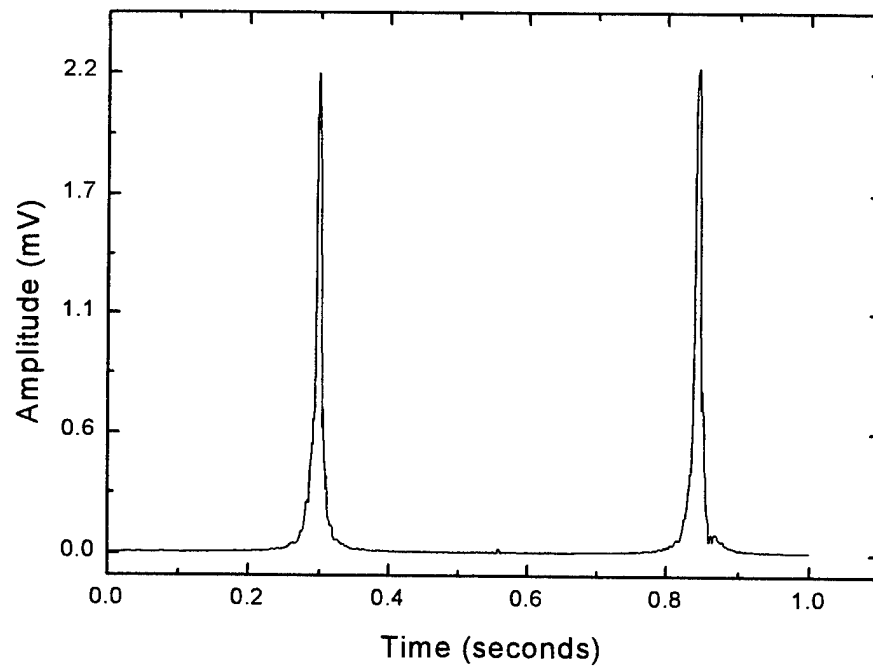


**Figure 4.7.** The unmodulated beam through the modulator. The FSR is 1.5 GHz.

Having established that the modulator was not adding structure to the spectral lines, the next step was to observe the spectral lines while the modulator operated at 125 MHz.

For AM modulation, the frequency spectrum consists of a center carrier frequency,  $\omega_c$ , with sidebands that are offset on either side of the carrier frequency by the sum and difference of the carrier with the modulation frequency,  $\omega_m$ . The amplitude of the sidebands of the AM signal is one-half the amplitude of the carrier times the fractional amount of modulation. This is depicted in Figure 4.8, and is mathematically described by Eqs (2.13)-(2.16).

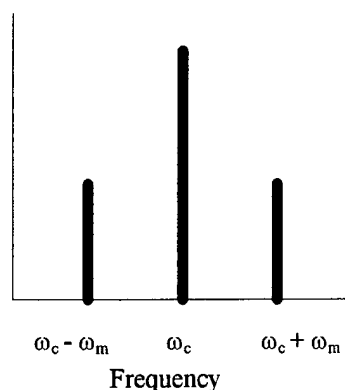


**Figure 4.8.** AM modulation spectrum. The carrier a frequency is  $\omega_c$ , and the modulation frequency is  $\omega_m$ . As depicted, the percent modulation is less than 100 %.

In our case, the carrier is an argon-ion laser beam. With either detector D1, D2, or D3, it is not feasible to measure the instantaneous amplitude of the optical wave, because the frequency of the carrier is  $5.8 \times 10^{14}$  Hz. Instead, D3 can respond to the modulated intensity of light up to frequencies of 300 MHz. The readout from D3 was measured directly from a Tektronix 2465 300 MHz oscilloscope, and the percentage of modulation was determined by dividing the peak voltage due to the modulation by the average voltage.

Because the beam routing in the experimental arrangement (Figure 3.1) made it impossible to simultaneously measure the modulation percentage and to view the spectrum, we first measured the percentage modulation from the oscilloscope readings, as stated above, and then inserted a mirror to redirect the beam path into the interferometer in order to observe and record the spectrum. This caused a delay of about 10 to 15 seconds between recording the modulation percentage and recording the frequency spectrum. However, this did not appear to be a significant problem.

With  $40 V_{p-p}$  at 125 MHz applied to the modulator, the ratio of the peak value for the signal from  $D_3$  to the average value for the signal from  $D_3$  predicted a modulation of 60%. Given the FSR of 1.5 GHz and 60% modulation, we expected to see sidebands appear in the observed spectrum with separation equal to the ratio of 125 MHz to the FSR, and with an amplitude equal to 30% of the main fringe. Figure 4.10 shows the spectrum for this level of modulation. The measured value of the amplitude of the sidebands is about 0.02mV, while the average value of the central peak is about 0.071 mV, corresponding to a ratio of the sideband amplitude to the central peak amplitude of 0.28, or a modulation of 56%. The difference may be accounted for by the fact that the signal from  $D_3$  was read off the oscilloscope, leading to not so precise determinations of the percent modulation.

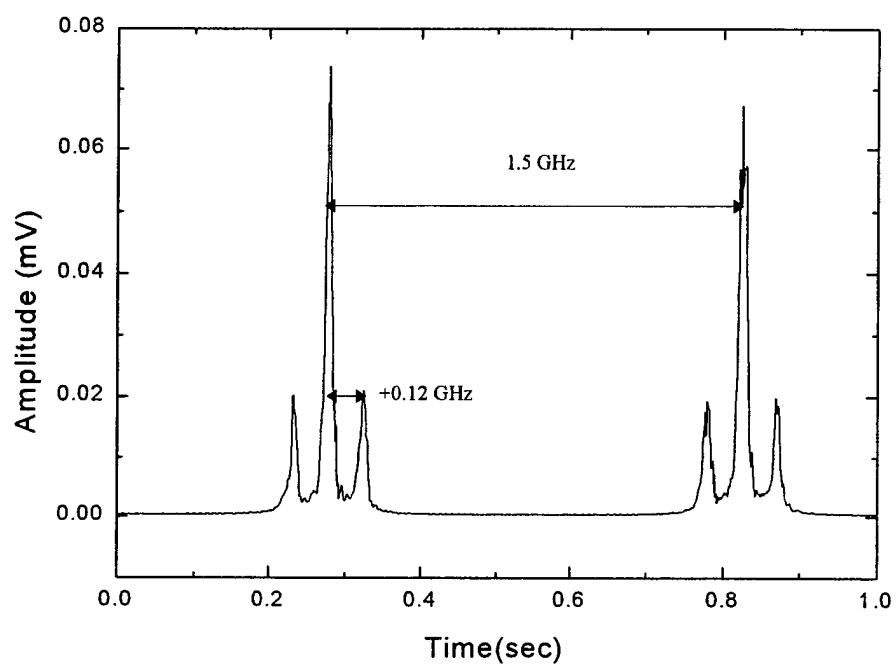


**Figure 4.10.** 60% modulation with 40  $V_{p-p}$  at 125 MHz.

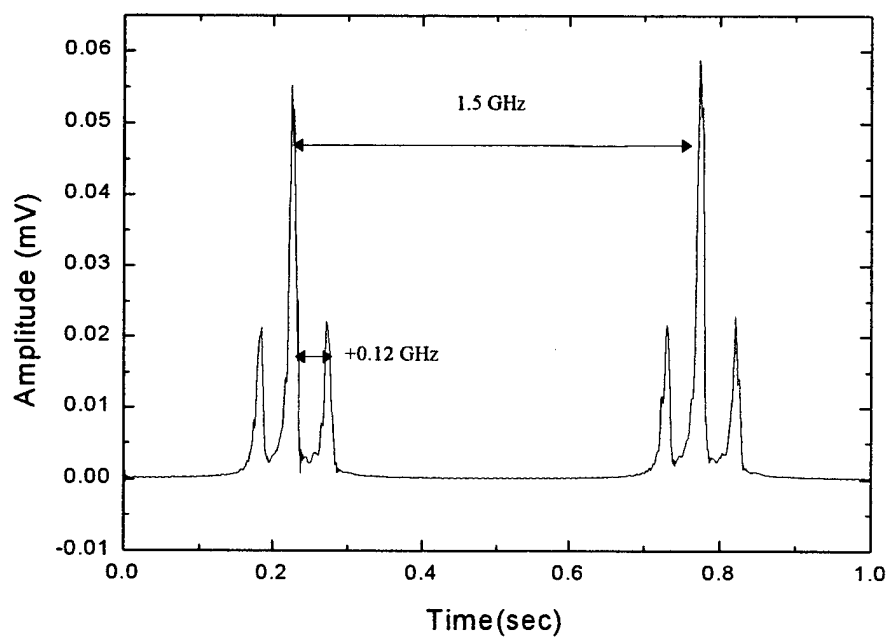


**Figure 4.11.** 80% modulation with 60  $V_{p-p}$  at 125 MHz.

For an applied signal of  $60 V_{p-p}$  at 125 MHz, the ratio of the peak value of the signal from  $D_3$  to the average value of the signal from  $D_3$  predicted 80% modulation. Therefore the observed amplitude of the sidebands was expected to be 0.4 times of the amplitude of the central peak with the same separation as those in Figure 4.10. Figure 4.11 shows the record of this modulation. The value of the central peak is about .057mV. The average value of the sideband is .023mV. This yields an observed ratio of 0.40, corresponding to the predicted 80% modulation.

## V. CONCLUSIONS AND RECOMMENDATIONS

We successfully characterized the performance of the LM 0202 P electro-optic modulator and achieved amplitude modulation of an argon ion laser at 125MHz. However, in order to do this we had to bias the quiescent point away from crossover point on the DC characteristic curve, which lowered the mean intensity of the transmitted beam. A high modulation of 80% was achieved, but only 7% of the beam was actually transmitted through the modulator.

When the electric field applied to the LM 0202P modulator was modulated at RF frequencies the effective parallel resistance of the electro-optic crystal is reduced. This is perhaps a result of dielectric losses in the crystal, which limits the modulator performance for modulating light near and about 100 MHz. Additional research may be conducted to determine the precise characteristic behavior profile of the modulator at various modulation frequencies. Nevertheless, there may be useful applications for this modulator at lower frequencies.



## LIST OF REFERENCES

1. Larraza and Coleman (1996), *Nonlinear Propagation in Optical Fibers: Applications to Tunable Lasers*, Andres Larraza, paper prepared for thesis students.
2. Michael C. Ladner (1996), *Optical Modulator LM 0202 P Characteristics: Application to Amplitude Modulation of Argon-Ion Laser*, Naval Postgraduate School.
3. Harlan Wallace (1996), *Optical Characteristics of the LEXEL 85 Argon-Ion Laser and Gsanger LM0202P Modulator: Application to AM-FM Light Conversion*, Naval Postgraduate School.
4. Mohammad A. Karim (1990), *Electro-Optical Devices and Systems*, PWS-KENT Publishing Company.
5. Amnon Yariv (1984), *Optical Waves in Crystals: Propagation and Control of Laser Radiation*, John Wiley and Sons, Inc.



## INITIAL DISTRIBUTION LIST

1. Defense Technical Information Center.....2  
8725 John J. Kingman Rd., STE 0944  
Ft. Belvoir, Virginia 22060-6218
  
2. Dudley Knox Library.....2  
Naval Postgraduate School  
411 Dyer Rd.  
Monterey, California 93943-5101
  
3. Dr. A. A. Atchley, Code PH/Ay.....1  
Department of Physics  
Naval Postgraduate School  
Monterey, California 93943-5002
  
4. Professor A. Larraza, Code PH/La.....2  
Department of Physics  
Naval Postgraduate School  
Monterey, California 93943-5002
  
5. Professor Scott Davis, Code PH/Dv.....2  
Department of Physics  
Naval Postgraduate School  
Monterey, California 93943-5002
  
6. Professor S. Gnanalingam, Code PH/Gm.....2  
Department of Physics  
Naval Postgraduate School  
Monterey, California 93943-5002
  
7. LT. John R. Tucker.....2  
5961 N. Brook Pl.  
Garden City, Idaho 83714